Synthesis of $LaTb_xO_y:Eu^{3+}$ nanowire arrays and study of performances on fluorescence enhancement and red shift

Qian Wang, Jie Feng, Guangzheng Peng, Tong Zhang, Ji Xiang, Peng Li, Lina Ye, Xiaoyou Yuan ✉

School of Chemistry and Chemical Engineering, Anhui University, Hefei 230601, People's Republic of China
✉ *E-mail: yuanxy@ahu.edu.cn*

Published in Micro & Nano Letters; Received on 29th December 2017; Revised on 18th March 2018; Accepted on 8th June 2018

Highly ordered $LaTb_xO_y:Eu^{3+}$ nanowire arrays have been synthesised in anodic aluminium oxide template by chemical co-deposition at negative pressure suction, it is amorphous and with homogeneous morphologies. There are two peaks at 619 and 704 nm with excitation wavelength of 394 nm, which have red shift slightly relative to the $^5D_0$–$^2F_2$ and $^5D_0$–$^7F_4$ energy level transition of Eu^{3+}, and Tb^{3+} exhibits strong fluorescence enhancement and sensitisation in $LaTb_xO_y:Eu^{3+}$ nanowire arrays with the existence of La^{3+}. The fluorescence intensity of $LaTb_xO_y:Eu^{3+}$ nanowire arrays is related to the doping concentration of Eu^{3+} ion. When the doping concentration of Eu^{3+} is 8%, the fluorescence intensity reaches a maximum, and remarkably decreases at higher concentrations.

1. Introduction: Recently, rare earth(RE) nanostructured materials have been intensively studied due to their potential applications in many fields such as optical display [1–5], medical imaging [6–11], gaseous sensor [12–16], bio-labelling [17–21] etc., all these come from the 4f electronic structure of RE element. It is well known that RE elements possess narrow bandgap between 4f and 5d orbits, and the 4f electrons can easily transfer to 5d orbit, which leads to various oxidation states and plentiful luminescent performances for RE elements. As a result, RE elements or RE compounds are usually qualified as luminescent host materials or luminescent material activators. Nowadays, RE oxide and doped RE oxide nanostructured materials have been widely studied due to their excellent bio-compatibility and non-poisonous advantage. As a result, RE oxide nanostructured materials can be used in medical optical display, biomedical engineering, and targeted drug deliver [22–33]. To make them applicable to the fields mentioned above, it is critical to construct the RE oxide nanostructures with highly ordered and homogeneous structure in precise dimensions. In fact, controllable synthesis is still the first goal for nanostructured materials and the prerequisite for applications in nanodevices.

In this Letter, highly ordered $LaTb_xO_y:Eu^{3+}$ nanowire arrays have been synthesised in anodic aluminium oxide (AAO) template by chemical co-deposition at negative pressure suction, and the synthesis process is discussed. The fluorescent performances of $LaTb_xO_y:Eu^{3+}$ nanowire arrays are investigated, and the results show it possesses the fluorescence emission in red light area, which is useful in medical imaging or cell labelling.

2. Experimental

2.1. Fabrication: An AAO template with nanopore diameter of 100 nm was first installed to a decompression pumping device and the gas tightness was checked. $RE(NO_3)_3$(RE = Tb, La, and Eu) solution and sodium hydroxide (NaOH) solution were prepared at 0.05, 0.05, 0.05, and 0.1 M. The mixed solution (in proportion) of $Tb(NO_3)_3$, $La(NO_3)_3$, $Eu(NO_3)_3$ and the NaOH solution were alternately dropped on the AAO template, and were immediately adhered to the nanopore walls of the AAO template by Coanda effect under the action of negative pressure. The nanopores of AAO template serve as nanoreactors. The precursor of hydroxide composed of terbium, lanthanum, and europium was obtained by the chemical co-deposition, which was annealed in a muffle furnace. The temperature was raised to 300°C at a heating rate of 1°C/min, maintained for 2 h, and then, naturally cooled to room temperature. The samples of $LaTb_xO_y:Eu^{3+}$ nanowire arrays wrapped up in AAO template were fabricated.

2.2. Characterisation: The samples of $LaTb_xO_y:Eu^{3+}$ nanowire arrays wrapped up in AAO template were first etched by 5 wt% NaOH solution for 5 min at room temperature to remove the partially AAO template, and washed by distilled water several times, then, dried in air and sprayed with gold for scanning electron microscopy (SEM) (S4800). Similarly, the samples were etched by 5 wt% NaOH solution for 10 min to isolate the $LaTb_xO_y:Eu^{3+}$ nanowire arrays from the AAO template, washed with distilled water, and then, dispersed in alcohol for transmission electron microscopy (TEM) (JEM-2100) characterisation. The structure and chemical composition of $LaTb_xO_y:Eu^{3+}$ nanowire arrays were characterised by X-ray diffraction (XRD) (MXP18AHF, Cu Kα, $\lambda = 1.5406$ Å) and energy dispersive X-ray analysis (EDS) (JEOL-2010), respectively. The fluorescence properties of the $LaTb_xO_y:Eu^{3+}$ nanowire arrays were measured by fluorescence spectrometer (PerkinElmer LS-55), xenon discharge lamp was used as the excitation light source and the excitation wavelength was 394 nm.

3. Results and discussion: Fig. 1 shows the SEM images of $LaTb_xO_y:Eu^{3+}$ nanowire arrays, front view in Fig. 1*a* and side view in Fig. 1*b*. These SEM images show that $LaTb_xO_y:Eu^{3+}$ nanowire arrays are highly ordered, uniform in size, and homogeneous structure in morphology, which could supply nanostructured material for biomedical engineering or nanodevice. Fig. 2 is TEM image of a single $LaTb_xO_y:Eu^{3+}$ nanowire, and the selected area electron diffraction (SAED) is inserted. The length of a single nanowire is about 5 μm and the diameter of $LaTb_xO_y:Eu^{3+}$ nanowire arrays are around 100 nm. To obtain uniform morphologies of $LaTb_xO_y:Eu^{3+}$ nanowire arrays, many influencing factors have to be taken into account such as concentration of reactants, suction pressure of decompression, heating rate, and thermal decomposition temperature etc. In fact, the concentrations of reactants should be much higher than that of the equilibrium concentration for solubility product constant (K_{sp}), which will ensure the precursor of

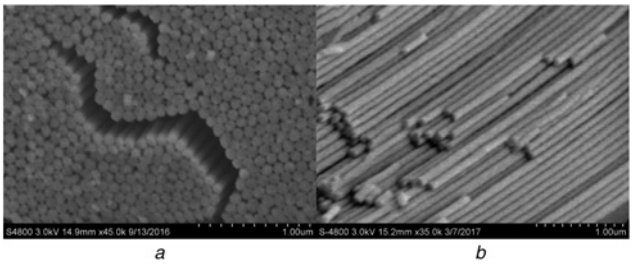

Fig. 1 *SEM image of $LaTb_xO_y$:Eu^{3+} nanowire arrays*
a Front view
b Side view

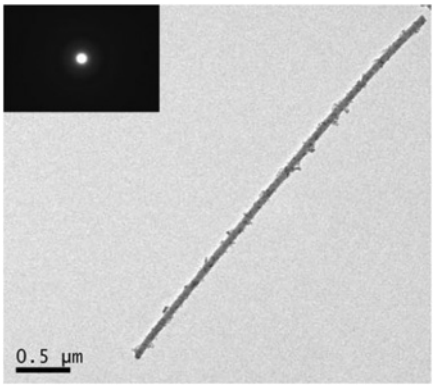

Fig. 2 *TEM image of $LaTb_xO_y$: Eu^{3+} nanowire, the inset image is SAED of $LaTb_xO_y$: Eu^{3+} nanowire*

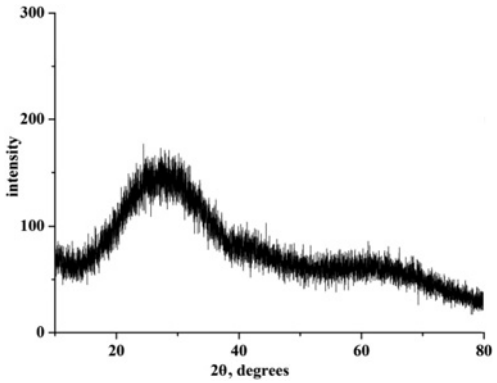

Fig. 3 *XRD spectrum of $LaTb_xO_y$: Eu^{3+} nanowire arrays*

hydroxide in amorphous structure, the aim of preparing amorphous $LaTb_xO_y$:Eu^{3+} nanowire arrays. However, if the concentrations of reactants are too large, the precursor of hydroxide will accumulate immediately in the surface of AAO template due to the fast reaction of chemical co-deposition, which blocked the reactants into the nanopores of AAO template, and the chemical co-deposition in nanopores will stop. For the suction pressure, 0.01 MPa suction pressure is suitable according to our experiments. If the vacuum degree is too high, the solution of reactants will quickly overflow the nanopores of AAO template, and no precursor of hydroxide was formed in the AAO template. To form a uniform and homogeneous nanostructure, the decomposition temperature and heating rate for the precursor of hydroxide should be carefully controlled, because there will be amount of H_2O to release during the process of thermal decomposition for the precursor. If the H_2O is released too fast, many defects will be left in the surface morphology of $LaTb_xO_y$:Eu^{3+} nanowires. The XRD spectrum of $LaTb_xO_y$:Eu^{3+} nanowire arrays is shown in Fig. 3, which is consistent with the SAED inserted in Fig. 2. The amorphous structure will ensure the uniformity of $LaTb_xO_y$:Eu^{3+} nanowire arrays in physical properties and avoid defects for anisotropy of crystal structure in optical display, which could extend their scope of applications. Fig. 4 is the EDS spectrum of $LaTb_xO_y$:Eu^{3+} nanowire arrays, which confirms the existence of terbium, lanthanum, and europium elements. The peaks of aluminium, oxygen, and platinum are from AAO template and the process of metal spraying.

The fluorescent spectra of $LaTb_xO_y$:Eu^{3+} nanowire arrays are shown in Fig. 5*a*. There are two emission peaks at 619 and 704 nm with excitation wavelength of 394 nm, which have red shift relative to the peaks of 615 and 702 nm corresponding to the $^5D_0$–$^2F_2$ and $^5D_0$–$^7F_4$ energy level transition of Eu^{3+}. Tb^{3+} exhibits strong fluorescence enhancement and sensitisation in $LaTb_xO_y$:Eu^{3+} nanowire arrays with the existence of La^{3+}. To study the fluorescence enhancement and sensitisation of Tb^{3+}, the fluorescent spectra of La_xO_y:Eu^{3+} nanowire arrays are investigated and shown in Fig. 5*b*. Compared to Figs. 5*a* and *b*, the fluorescence intensity of $LaTb_xO_y$:Eu^{3+} nanowire arrays is much stronger than that of the La_xO_y:Eu^{3+}, the fluorescence enhancement and sensitisation of Tb^{3+} are obvious in $LaTb_xO_y$:Eu^{3+} nanowire arrays. Meanwhile, lanthanum, as a matrix, plays a key role of stabilising the luminescent properties in $LaTb_xO_y$:Eu^{3+} nanowire arrays. In addition, the fluorescence intensity of $LaTb_xO_y$:Eu^{3+} nanowire arrays is related to the doping concentration of Eu^{3+}. When the doping concentration of Eu^{3+} is 8%, the fluorescence intensity reaches a maximum, and remarkably decreases at higher concentrations. It may be a result of fluorescence quenching related to the lattice deformation, which in turn is determined by the concentration of Eu^{3+} ions in the lattice.

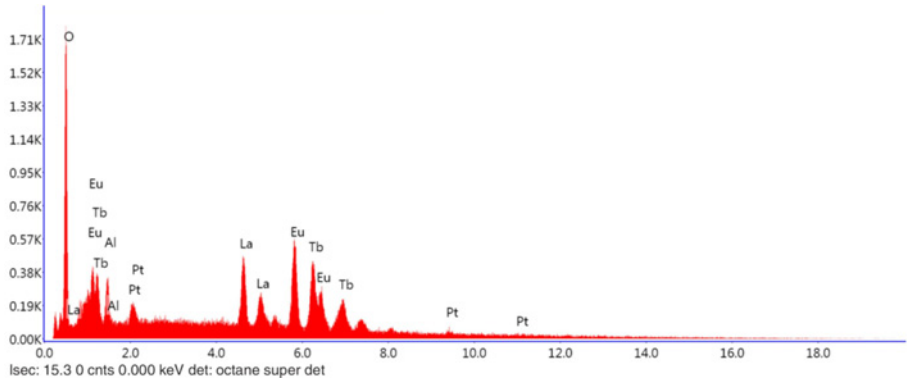

Fig. 4 *EDS spectrum of $LaTb_xO_y$: Eu^{3+} nanowire arrays*

doi: 10.1049/mnl.2017.0923

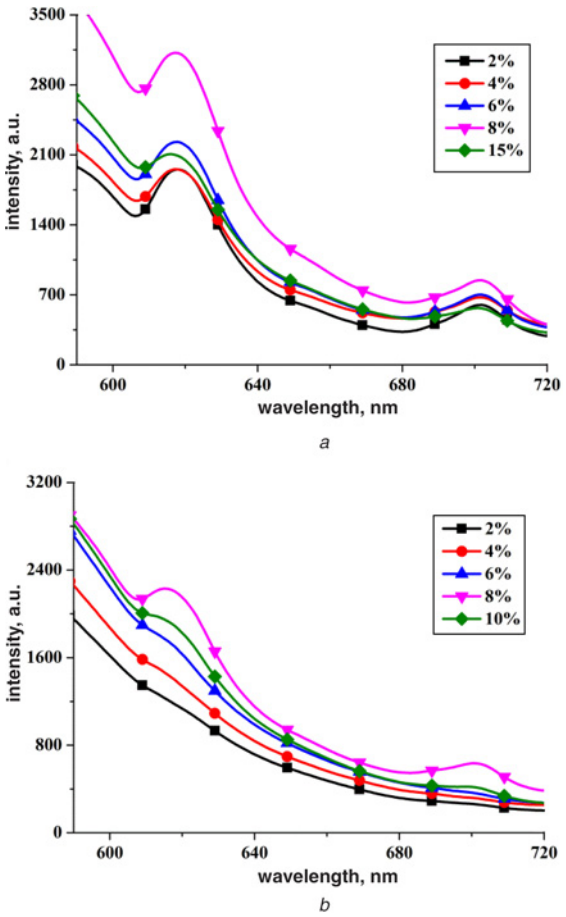

Fig. 5 *Fluorescence spectra*
a $LaTb_xO_y$: Eu^{3+} nanowire arrays
b La_xO_y: Eu^{3+} nanowire arrays

4. Conclusions: Highly ordered $LaTb_xO_y$:Eu^{3+} nanowire arrays have been synthesised in AAO template by chemical co-deposition at negative pressure suction, which are amorphous, and possess precise dimension and homogeneous morphologies. There are two emission peaks at 619 and 704 nm with excitation wavelength of 394 nm, which have red shift relative to the peaks of 615 and 702 nm corresponding to the $^5D_0$–$^2F_2$ and $^5D_0$–$^7F_4$ energy level transition of Eu^{3+}. Tb^{3+} exhibits strong fluorescence enhancement and sensitisation in $LaTb_xO_y$:Eu^{3+} nanowire arrays with the existence of La^{3+}. The doping concentration of Eu^{3+} influences the fluorescence intensity of $LaTb_xO_y$:Eu^{3+} nanowire arrays, which reaches a maximum with doping concentration of Eu^{3+} at 8%, and remarkably decreases at higher doping concentrations.

5. Acknowledgment: This work was supported by the National Natural Science Foundation of China (grant no. 51472001).

6 References

[1] Hou D.J., Guo X.X., Liu C.M., *ET AL.*: 'Hydrothermal synthesis, X-ray absorption and luminescence properties of Tb^{3+} doped $LaPO_4$', *J. Lumin.*, 2015, **165**, pp. 23–29
[2] Thummavichai K., Wang N.N., Cheong Lem L., *ET AL.*: 'Lanthanide-doped $W_{18}O_{49}$ nanowires: synthesis, structure and optical properties', *Mater. Lett.*, 2018, **214**, pp. 232–235
[3] Wang F.K., Yuan X.Y., Li P.: 'Fabrication, magnetic anisotropy and tunable fluorescence of amorphous $La_xCu_yO_z$ nanowire arrays', *Mater. Lett.*, 2014, **126**, pp. 39–42
[4] Yu H.Q., Li Y., Song Y., *ET AL.*: 'Preparation and luminescent properties of Gd_2O_3:Eu^{3+} nanofibres made by electrospinning', *Ceram. Int.*, 2016, **42**, pp. 1307–1313
[5] Wu K.L., Liu K., Wei X.W., *ET AL.*: 'Ce^{3+}-doped neodymium phosphate nanostructures: controllable synthesis, influencing factors, and photoluminescence properties', *Micro Nano Lett.*., 2016, **11**, (1), pp. 57–61
[6] Cui X.J., Mathe D., Kovacs N., *ET AL.*: 'Synthesis, characterization, and application of core-shell $Co_{0.16}Fe_{2.84}O_4$@$NaYF_4$(Yb, Er) and Fe_3O_4@$NaYF_4$(Yb, Tm) nanoparticle as trimodal (MRI, PET/SPECT, and optical) imaging agents', *Bioconjugate Chem.*, 2016, **27**, (2), pp. 319–328
[7] Park Y.I., Kim H.M., Kim J.H., *ET AL.*: 'Theranostic probe based on lanthanide-doped nanoparticles for simultaneous in vivo dual-modal imaging and photodynamic therapy', *Adv. Mater.*, 2012, **24**, (42), pp. 5755–5761
[8] Wang F., Yang B., Chen X.M., *ET AL.*: 'Color-tunable and upconversion luminescence of Gd_2O_2S:Er,Tb phosphor', *Mater. Chem. Phys.*, 2016, **169**, pp. 113–119
[9] Xu J.T., Yang P.P., Sun M.D., *ET AL.*: 'Highly emissive dye-sensitized upconversion nanostructure for dual-photosensitizer photodynamic therapy and bioimaging', *ACS Nano*, 2017, **11**, (4), pp. 4133–4144
[10] Xu J.T., Gulzar A., Liu Y.H., *ET AL.*: 'Integration of IR-808 sensitized upconversion nanostructure and MoS_2 nanosheet for 808 nm NIR light triggered phototherapy and bioimaging', *Small*, 2017, **13**, (36), pp. 1701841–1701853
[11] Xu J.T., He F., Cheng Z.Y., *ET AL.*: 'Yolk-structured upconversion nanoparticles with biodegradable silica shell for FRET sensing of drug release and imaging-guided chemotherapy', *Chem. Mater.*, 2017, **29**, (17), pp. 7615–7628
[12] Ding D.G., Lu W.B., Xiong Y., *ET AL.*: 'Facile synthesis of $La_2O_2CO_3$ nanoparticle films and its CO_2 sensing properties and mechanisms', *Appl. Surf. Sci.*, 2017, **426**, pp. 725–733
[13] Michel C.R., Martínez-Preciado A.H.: 'CO sensing properties of novel nanostructured La_2O_3 microspheres', *Sens. Actuators B, Chem.*, 2015, **208**, pp. 355–362
[14] Sanal Kumar G., Illyaskutty N., Suresh S., *ET AL.*: 'Terbium oxide doped MoO_3 nanostructures: morphology engineering and enhanced photoluminescence', *J. Alloys Compd.*, 2017, **698**, pp. 215–227
[15] Yadav A.A., Lokhande A.C., Kim J.H., *ET AL.*: 'Enhanced sensitivity and selectivity of CO_2 gas sensor based on modified La_2O_3 nanorods', *J. Alloys Compd.*, 2017, **723**, pp. 880–886
[16] Zhang P.P., Qin H.W., Zhang H., *ET AL.*: 'CO_2 gas sensors based on $Yb_{1-x}Ca_xFeO_3$ nanocrystalline powders', *J. Rare Earths*, 2017, **35**, (6), pp. 602–609
[17] Bai H.Y., Song Y., Li D., *ET AL.*: 'Emerging $La_2O_2CN_2$ matrix with controllable 3D morphology for photoluminescence applications', *CrystEngComm*, 2017, **19**, (43), pp. 6498–6505
[18] Chinen A.B., Guan C.M., Ferrer J.R., *ET AL.*: 'Nanoparticle probes for the detection of cancer biomarkers, cells, and tissues by fluorescence', *Chem. Rev.*, 2015, **115**, (19), pp. 10530–10574
[19] Ma X., Liu Y., Wu X.M., *ET AL.*: 'Synthesis of europium-doped nanohydroxyapatite and its cytocompatibility with endothelial cells in vitro', *Mater. Technol.*, 2016, **31**, (sup 1), pp. 23–27
[20] Li J.G., Wang X.J., Liu W.G., *ET AL.*: '$(La_{0.97}RE_{0.01}Yb_{0.02})_2O_2S$ nanophosphors converted from layered hydroxyl sulfate and investigation of upconversion photoluminescence (RE = Ho, Er)', *Nanoscale Res. Lett.*, 2017, **12**, (1), p. 508
[21] Wang M., Li M., Yu A.Y., *ET AL.*: 'Rare earth fluorescent nanomaterials for enhanced development of latent fingerprints', *ACS Appl. Mater. Interfaces*, 2015, **7**, (51), pp. 28110–28115
[22] Bünzli J.-C.G.: 'Lanthanide light for biology and medical diagnosis', *J. Lumin.*, 2016, **170**, pp. 866–878
[23] Chall S., Mati S.S., Gorain B., *ET AL.*: 'Toxicological assessment of PEG functionalized f-block rare earth phosphate nanorods', *Toxicol. Res.*, 2015, **4**, (4), pp. 966–975
[24] Gao J., Li R.B., Wang F.B., *ET AL.*: 'Determining the cytotoxicity of rare earth element nanoparticles in macrophages and the involvement of membrane damage', *Environ. Sci. Technol.*, 2017, **51**, (23), pp. 13938–13948
[25] Gnach A., Lipinski T., Bednarkiewicz A., *ET AL.*: 'Upconverting nanoparticles: assessing the toxicity', *Chem. Soc. Rev.*, 2015, **44**, (6), pp. 1561–1584
[26] Saraf M., Kumar P., Kedawat G., *ET AL.*: 'Probing highly luminescent europium-doped lanthanum orthophosphate nanorods for strategic applications', *Inorg. Chem.*, 2015, **54**, (6), pp. 2616–2625
[27] Singh L.P., Singh N.P., Srivastava S.K.: 'Terbium doped SnO_2 nanoparticles as white emitters and SnO_2:5Tb/Fe_3O_4 magnetic luminescent nanohybrids for hyperthermia application and biocompatibility with HeLa cancer cells', *Dalton Trans.*, 2015, **44**, (14), pp. 6457–6465

[28] Teo R.D., Termini J., Gray H.B.: 'Lanthanides: applications in cancer diagnosis and therapy', *J. Med. Chem.*, 2016, **59**, (13), pp. 6012–6024
[29] Tian J., Zeng X., Xie X.J., *ET AL.*: 'Intracellular adenosine triphosphate deprivation through lanthanide-doped nanoparticles', *J. Am. Chem. Soc.*, 2015, **137**, (20), pp. 6550–6558
[30] Tian Y., Fu Y., Xing M.M., *ET AL.*: 'Upconversion luminescence properties of Y_2O_3:Yb, Er and Y_2O_2S:Yb, Er nanoparticles prepared by complex precipitation', *J. Nanomater.*, 2015, **2015**, pp. 1–7
[31] Wang H.Q., Tu D.T., Xu J., *ET AL.*: 'Lanthanide-doped LaOBr nanocrystals: controlled synthesis, optical spectroscopy and bioimaging', *J. Mater. Chem. B*, 2017, **5**, (25), pp. 4827–4834
[32] Zheng W., Tu D.T., Huang P., *ET AL.*: 'Time-resolved luminescent biosensing based on inorganic lanthanide-doped nanoprobes', *Chem. Commun.*, 2015, **51**, (20), pp. 4129–4143
[33] Wang F.K., Yuan X.Y.: 'Growth process and magnetic anisotropy of amorphous $La_xZn_yO_z$ nanowire arrays', *Micro Nano Lett.*, 2014, **9**, (4), pp. 222–224

doi: 10.1049/mnl.2017.0923